3. Subbarao P, Stanojevic S, Brown M, Jensen R, Rosenfeld M, Davis S, Brumback L, Gustafsson P, Ratjen F. Lung clearance index as an outcome measure for clinical trials in young children with cystic fibrosis: a pilot study using inhaled hypertonic saline. *Am J Respir Crit Care Med* 2013;188:456–460.
4. Milla CE, Ratjen F, Marigowda G, Liu F, Waltz D, Rosenfeld M; VX13-809-011 Part B Investigator Group. Lumacaftor/ivacaftor in patients aged 6–11 years with cystic fibrosis homozygous for F508del-CFTR. *Am J Respir Crit Care Med* 2017;195:912–920.
5. Wielpütz MO, Puderbach M, Kopp-Schneider A, Stahl M, Fritzsching E, Sommerburg O, Ley S, Sumkauskaite M, Biederer J, Kauczor HU, *et al*. Magnetic resonance imaging detects changes in structure and perfusion, and response to therapy in early cystic fibrosis lung disease. *Am J Respir Crit Care Med* 2014;189:956–965.
6. Thomen RP, Walkup LL, Roach DJ, Cleveland ZI, Clancy JP, Woods JC. Hyperpolarized (129)Xe for investigation of mild cystic fibrosis lung disease in pediatric patients. *J Cyst Fibros* 2017;16:275–282.
7. Rayment J, Kanhere N, Kowalik K, Couch M, Kavanagh B, Ratjen F, Santyr G. Correlation of lung clearance index with hyperpolarized 129Xe pulmonary MRI in pediatric cystic fibrosis [abstract]. *Pediatr Pulmonol* 2016;51:S286.
8. Walkup LL, Thomen RP, Bell E, Decker B, Cleveland Z, Clancy JP, Woods JC. Quantification of regional ventilation heterogeneity of early cystic fibrosis lung disease via 129xe magnetic resonance imaging: comparison with PFT and LCI [abstract]. *Pediatr Pulmonol* 2016;51:S351.
9. Kirby M, Heydarian M, Svenningsen S, Wheatley A, McCormack DG, Etemad-Rezai R, Parraga G. Hyperpolarized 3He magnetic resonance functional imaging semiautomated segmentation. *Acad Radiol* 2012; 19:141–152.
10. Walkup LL, Thomen RP, Akinyi TG, Watters E, Ruppert K, Clancy JP, Woods JC, Cleveland ZI. Feasibility, tolerability and safety of pediatric hyperpolarized (129)Xe magnetic resonance imaging in healthy volunteers and children with cystic fibrosis. *Pediatr Radiol* 2016;46:1651–1662.
11. Gustafsson PM, Robinson PD, Gilljam M, Lindblad A, Houltz BK. Slow and fast lung compartments in cystic fibrosis measured by nitrogen multiple-breath washout. *J Appl Physiol (1985)* 2014;117:720–729.
12. Horn FC, Deppe MH, Marshall H, Parra-Robles J, Wild JM. Quantification of regional fractional ventilation in human subjects by measurement of hyperpolarized 3He washout with 2D and 3D MRI. *J Appl Physiol (1985)* 2014;116:129–139.

Right Ventricle Vasculature in Human Pulmonary Hypertension Assessed by Stereology

To the Editor:

There is growing interest in the potential vascular rarefaction of the right ventricular (RV) microcirculation to explain RV failure due to pulmonary hypertension (PH). Published data, reliant on measures of stained capillary area in selected RV fields, indicated a potential capillary drop, possibly of 50 or 60% versus control values, in decompensated RVs in PH induced by SU5416-hypoxia and monocrotaline (1, 2); supportive qualitative data were reported in human RV by immunostaining (2). However, accurate assessment of the vasculature in the normal and diseased RV requires an unbiased approach, with tools including systematic uniform random sampling and assessment of the pertinent reference volume (i.e., RV tissue) (3). Using these approaches, the hypoxia mouse and SU5416-hypoxia rat models of PH exhibited increased absolute vascular length that parallels the increase in RV cell mass (4, 5), leading to maintenance of the ratio between myocyte volume and capillary length. In this pilot study, we report a systematic unbiased analysis of human RV specimens using a rigorous stereologic approach. Our data indicate that in advanced PH, there was a significant increase of the RV vasculature, whereas the average radius of RV myocyte served per vessel increased by 17% over control subjects.

Methods

All studies were approved by the Colorado Multiple Institutional Review Board (Protocol #08-0462). Cardiac tissue was collected at autopsy and processed by sectioning the heart in 1-cm-thick slices (Figure 1A), starting at the apex, at a depth between 1 and 10 mm as determined by computerized random number generator, and continued every 1 cm to the atrioventricular junction. The slices were laid down and imaged adjacent to a ruler. A plastic sheet with 5-mm holes at 1-cm intervals was placed over the tissue. Eight uniformly random locations were identified, with a random start for the first location (determined by computerized random number generator) and at regular intervals thereafter (6). Each location was marked with ink, and a 5-mm core biopsy was performed at each site. Isotropic orientation of the biopsies was performed with the Isector technique (7), with each sample formalin-fixed and embedded in a paraffin ball, which was rolled. In the final orientation, the ball was placed into a

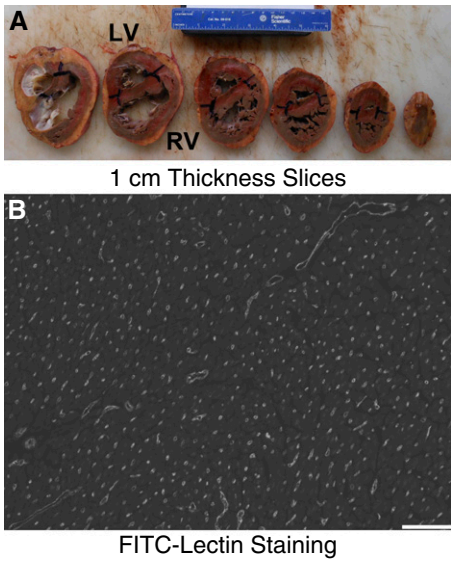

Figure 1. Stereologic approach for analysis of right ventricle (RV) vasculature. (*A*) The ventricles are sectioned at 1-cm thickness with a random start. (*B*) Uniform, random, isotropically oriented sections are stained with fluorescein isothiocyanate–lectin (FITC-Lectin) (*scale bar*: 100 μm). LV = left ventricle.

Supported by National Institutes of Health grants P01HL014985 (B.B.G. and R.M.T.), K08HL105536, R03HL133306, and R01HL135872; the University of Colorado Department of Medicine Early Career Scholars Program (B.B.G.); and grant R24HL123767 (R.M.T.).

Author Contributions: Conception and design: B.B.G. and R.M.T.; tissue collection and processing: D.K., B.K., and R.M.T.; analysis and interpretation: B.B.G. and R.M.T.; drafting the manuscript for important intellectual content: B.B.G. and R.M.T.; approval of the final manuscript: all authors.

Originally Published in Press as DOI: 10.1164/rccm.201702-0425LE on March 9, 2017

slicer matrix (Zivic, Pittsburgh, PA) for cutting into 3-mm interval slices. Slices with tissue were laid down, reembedded into a paraffin block, and sectioned at 4 μm.

RV absolute volume was calculated using Cavalieri's method on the fresh tissue image (8). The outline of the RV tissue was drawn (Photoshop; Adobe, San Jose, CA), and cross-sectional area determined. The absolute volume was calculated as the sum of RV cross-sectional areas multiplied by the slice thicknesses (1 cm).

Each section underwent antigen retrieval (Vector H3300; Vector Laboratories, Burlingame, CA), Tris-buffered saline with Tween 20 rinse, staining overnight at 4°C with fluorescein isothiocyanate–labeled lectin from *Griffonia simplicifolia* (Sigma L9381; Sigma-Aldrich, St. Louis, MO; 1:75 dilution in Tris-buffered saline), and coverslipping (Vector H1400). Four images of each section were randomly acquired using a microscope (Nikon, Tokyo, Japan) with a black-and-white camera (Photometrics, Tucson, AZ) (Figure 1B). Two specimens had poor lectin signal, and anti-CD31 immunostaining (ab28364; Abcam, Cambridge, MA) was performed instead.

Vascular length (L_v) was determined using the equation $L_v = 2Q/AP$ (9, 10), where Q is the sum of vessel profiles that intersect a test plane, P is the sum of test points that intersect the tissue, and A is the plane area divided by the number of test points. The test plane we used had a sampling area of 0.550 mm^2 and 1,426 test points, for an A of 386 μm^2.

Each image was digitally thresholded (Metamorph; Molecular Devices, Sunnyvale, CA) on tissue autofluorescence to identify all RV tissue and determine P. The image was then rethresholded on the lectin signal, and the number of vessel profiles Q that intersected the test plane (but not the exclusion boundary) was determined. The sum of all Ps and all Qs for each specimen was used to calculate L_v. L_v was corrected for tissue shrinkage by formalin fixation (estimated at 20% for each dimension, although variability in this factor may introduce bias [3]). L_v was multiplied by absolute volume to determine absolute vascular length for each specimen.

We also calculated the average cross-sectional area of cardiac tissue supplied by a single vessel, or volume of tissue per vessel length ($1/L_v$), and then the effective radius of tissue supplied by each vessel ($r = \sqrt{1/\pi L_v}$).

Results

Tissue was collected and analyzed from three control subjects and four subjects with advanced PH. Absolute RV volume, absolute length of the vasculature in the RV, and the average radius of RV tissue served per vessel were determined (Figure 2). Total vascular length in the RV tissue was highly correlated with absolute RV volume across all control and PH specimens ($P < 0.001$). The average radius of tissue served per vessel was 14.4 μm in control RVs and 16.9 μm in PH RVs ($P < 0.05$).

Discussion

We applied a stringent stereologic approach to analyze human RV vasculature, in line with American Thoracic Society guidelines for stereological assessment of lung structure (3). This approach is similar to that previously reported in the hypoxic mouse and SU5416-hypoxia rat models (4, 5).

In this pilot study, we observed a strong correlation between total vascular length and myocyte volume, consistent with significant compensatory angiogenesis in the PH RV. This likely occurs in homeostatic adaptation to support RV contractile function in the setting of increased afterload and muscle mass.

We observed a 2.5-μm increase in the radius of tissue supplied by each vessel, consistent with vascular rarefaction in these terminal disease samples. This increase is smaller than a predicted 9.3-μm increase in radius if there was no vascular adaptation and RV volume increased 2.7-fold (the average we observed), or a predicted 6.0-μm increase in radius if there was actually 50% dropout of vessels, as suggested by prior planimetric analyses (1, 2). We suspect a 2.5-μm increase in radius is unlikely to significantly limit O_2 delivery but cannot exclude a restriction of other metabolite transport to the cardiomyocytes.

The importance of these data requires confirmation with a larger number of specimens and reinforces the need for application of rigorous stereologic techniques for unbiased tissue characteristic analysis. ■

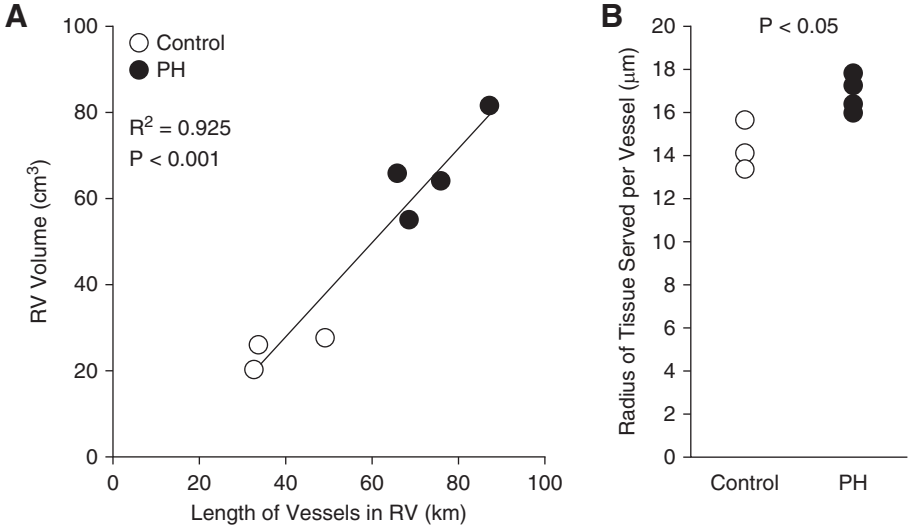

Figure 2. Analysis of right ventricle (RV) vessels in three control and four pulmonary hypertension (PH) specimens. (*A*) Total RV volume, measured by Cavalieri's method, versus absolute length of vessels in the RV tissue, measured by stereology (n = 3–4/group; linear regression). (*B*) Average radius of RV tissue served per vessel (n = 3–4/group; *t* test).

Author disclosures are available with the text of this letter at www.atsjournals.org.

Brian B. Graham, M.D.
Dan Koyanagi, B.S.
Balasubramaniyam Kandasamy, M.D.
Rubin M. Tuder, M.D.
Anschutz Medical Campus
Aurora, Colorado

References

1. Bogaard HJ, Natarajan R, Henderson SC, Long CS, Kraskauskas D, Smithson L, Ockaili R, McCord JM, Voelkel NF. Chronic pulmonary artery pressure elevation is insufficient to explain right heart failure. *Circulation* 2009;120:1951–1960.
2. Piao L, Fang YH, Parikh K, Ryan JJ, Toth PT, Archer SL. Cardiac glutaminolysis: a maladaptive cancer metabolism pathway in the right ventricle in pulmonary hypertension. *J Mol Med (Berl)* 2013;91:1185–1197.
3. Hsia CCW, Hyde DM, Ochs M, Weibel ER; ATS/ERS Joint Task Force on Quantitative Assessment of Lung Structure. An official research policy statement of the American Thoracic Society/European Respiratory Society: standards for quantitative assessment of lung structure. *Am J Respir Crit Care Med* 2010;181:394–418.
4. Kolb TM, Peabody J, Baddoura P, Fallica J, Mock JR, Singer BD, D'Alessio FR, Damarla M, Damico RL, Hassoun PM. Right ventricular angiogenesis is an early adaptive response to chronic hypoxia-induced pulmonary hypertension. *Microcirculation* 2015;22:724–736.
5. Zhang L, Perez M, Serkova N, Graham B, Tuder RM. Preservation of capillary network of the right ventricle in severe experimental pulmonary hypertension. *Pulm Circ* 2013;3:185.
6. Herring MJ, Putney LF, Wyatt G, Finkbeiner WE, Hyde DM. Growth of alveoli during postnatal development in humans based on stereological estimation. *Am J Physiol Lung Cell Mol Physiol* 2014;307:L338–L344.
7. Hyde DM, Harkema JR, Tyler NK, Plopper CG. Design-based sampling and quantitation of the respiratory airways. *Toxicol Pathol* 2006;34:286–295.
8. Gundersen HJ, Jensen EB. The efficiency of systematic sampling in stereology and its prediction. *J Microsc* 1987;147:229–263.
9. Howard CV, Reed MG. Unbiased stereology: three-dimensional measurement in microscopy. 2nd ed. Abingdon: BIOS Scientific Publishers; 2005.
10. Mühlfeld C. Quantitative morphology of the vascularisation of organs: a stereological approach illustrated using the cardiac circulation. *Ann Anat* 2014;196:12–19.

Increased CD13 Expression in Acute Myeloid Leukemia–associated Early Acute Hypoxic Respiratory Failure

To the Editor:

Acute myeloid leukemia (AML) is the most frequent acute leukemia in adults, and acute hypoxemic respiratory failure is a major cause of mortality during its early phase (1). Severe cases of leukemia-specific acute hypoxic respiratory failure (LS-ARF) include pulmonary leukostasis, lung leukemic infiltration, acute lysis pneumopathy, and differentiation syndrome and present with severe hypoxemia requiring mechanical ventilation and bilateral pulmonary infiltrates on chest imaging mimicking acute respiratory distress syndrome (ARDS). Although the expression of characteristic immunophenotypic markers by leukemic cells, as measured by flow cytometry, has been associated with decreased overall survival during AML (2), no study has investigated the association between flow cytometry markers and LS-ARF. Two observations suggest such association: first, CD11b/CD18 is involved in the pathogenesis of leukostasis (3), and second, certain AML subtypes (myelomonocytic or monocytic) are more specifically associated with respiratory complications (4) and have distinctive flow cytometry markers. We hypothesized that leukemic cell flow cytometry markers are associated with LS-ARF during the early phase of AML.

After institutional review board approval, we analyzed flow cytometry and clinical data in patients with newly diagnosed AML admitted between 2012 and 2015, according to the development of LS-ARF within 15 days of diagnosis. To define LS-ARF, we included patients diagnosed with pulmonary leukostasis, lung leukemic infiltration, acute lysis pneumopathy, or differentiation syndrome on the basis of previously published criteria (1, 5) who also fulfilled ARDS criteria (6). Flow cytometry was performed on bone marrow using a six-color BD FACSCanto I flow cytometer (BD Biosciences, San Jose, CA). Data for selected antibodies (CD14, CD64, CD11c, CD13, and anti–human leukocyte antigen DR, CD45) were analyzed using FCSExpress Software v3 (De Novo Software, Thornhill, Ontario, Canada). A gate of all $CD45^{+}$ events excluding lymphocytes and debris was established for each patient, and cells in the gate were determined to be positive or negative on the basis of quadrant gates set using cells stained with CD45 only as negative control. This allowed us to most closely reflect the entire neoplastic cell population and to obtain the most consistently reproducible denominator for our analysis. This population encompassed the traditional blast, maturing granulocyte, and maturing monocyte gates by CD45 versus side scatter, and excluded lymphocytes, nucleated erythroblasts, unlysed anucleate erythrocytes, platelets, and cellular debris. These populations were excluded, as they represent nonneoplastic cells and/or confounding events. We collected the percentage of positive cells and the mean fluorescent intensities for each antigenic marker. Results are presented as median (range), and nonparametric statistical tests (Fisher exact test, Mann-Whitney *U* test) were used to compare patients' characteristics according to the presence of LS-ARF.

Eight patients who developed LS-ARF within 15 days were compared with 92 patients without LS-ARF. The presumed etiologies and timing of LS-ARF were as follows: pulmonary leukostasis (Day 1 for three patients), lung leukemic infiltration (Day 3, Day 7, Day 10), acute lysis pneumopathy (Day 13 for the only patient who received chemotherapy before LS-ARF) and differentiation syndrome (Day 2). Two patients with leukostasis also presented with laboratory tumor lysis syndrome on admission. Six of the eight patients with LS-ARF had chest computed tomography scans showing multifocal bilateral airspace opacities (n = 5), diffuse bilateral ground-glass opacities (n = 3), and pleural effusion (n = 4). Clinical and flow cytometry data are detailed in Table 1. Patients with LS-ARF had higher white blood cells (WBC) count on admission and a higher Day 28 mortality, but other demographic and clinical characteristics, including FAB (French-American-British classification) M4/5 subtypes,

Author Contributions: C.S., M.B., D.C. and A.V.d.L. designed the study; C.S., C.B., and R.D. collected the data; C.S., M.B., C.B., and A.V.d.L. analyzed the data; C.S. and A.V.d.L. drafted the manuscript. All authors approved the final manuscript.

Originally Published in Press as DOI: 10.1164/rccm.201701-0080LE on March 21, 2017